

This is the peer-reviewed version of the following article:

Quinone-Decorated Onion-Like Carbon/Carbon Fiber Hybrid Electrodes for High-Rate Supercapacitor Applications

Marco Zeiger, Daniel Weingarth, and Volker Presser

ChemElectroChem 2(8)

Keywords:

binder-free electrodes, carbon, quinones, rate handling, supercapacitors

It has been published in final form at <http://dx.doi.org/10.1002/celc.201500130>.
This article may be used for non-commercial purposes in accordance with Wiley Terms and Conditions for Self-Archiving.

DOI: 10.1002/ ((please add manuscript number))

Full Paper

Quinone-decorated onion-like carbon / carbon fiber hybrid electrodes for high rate supercapacitor applications

*Marco Zeiger, Daniel Weingarth, and Volker Presser**

M. Zeiger, Prof. Dr. V. Presser

INM - Leibniz Institute for New Materials, Campus D2 2, 66123 Saarbrücken, Germany
& Department of Materials Science and Engineering, Saarland University, Campus D2 2,
66123 Saarbrücken, Germany

E-mail: volker.presser@inm-gmbh.de

Dr. D. Weingarth

INM - Leibniz Institute for New Materials, Campus D2 2, 66123 Saarbrücken, Germany

Keywords: supercapacitor, carbon onions, quinones, binder-free, rate handling

Abstract:

The energy performance of carbon onions can significantly be enhanced by introducing pseudocapacitive materials, but commonly at the cost of power handling. In this study a novel, synergistic electrode preparation method was developed using carbon fiber substrates loaded with quinone-decorated carbon onions. The electrodes are free-standing, binder-free, extremely conductive, and the interfiber space filling overcomes the severely low apparent density commonly found for electrospun fibers. Electrochemical measurements were performed in organic and aqueous electrolyte. For both systems a high electrochemical stability after 10,000 cycles was measured as well as a long-time voltage floating test for the organic electrolyte. The capacitance in 1 M H₂SO₄ was 288 Fg⁻¹ for the highest loading with quinones, similar to literature values, but with an ultrafast power handling showing more than 100 Fg⁻¹ at 2 Vs⁻¹ scan rate.

1. Introduction

Electrical double-layer capacitors (EDLCs), or supercapacitors, are energy storage devices with high power density compared to other electrochemical energy storage technologies.^[1-3] This high power handling is accomplished by the physical energy storage mechanism of highly efficient ion electrosorption at the interface of an electrolyte with high surface area carbon electrodes.^[1, 2] However, EDLCs show a very moderate energy density compared to batteries with the latter capitalizing electrochemical redox reactions and current research efforts target to overcome this limitation.^[4, 5] Most commonly, EDLC electrodes are composed of activated carbons (AC) considering its moderate-to-low cost and high natural abundance of AC organic precursors.^[6] In addition, a plethora of other carbon materials has been explored, such as carbon nanotubes,^[7] graphene,^[8] carbide-derived carbon,^[9] templated carbons,^[10] carbon black,^[11] and carbon onions.^[1, 12]

Carbon onions, also known as onion-like carbon (OLC), are an intriguing class of carbon nanomaterial that consists of spherical carbon nanoparticles that can be seen as mostly sp^2 -hybridized multishell fullerenes.^[13] OLC has been investigated as a promising material for extremely high power handling applications^[14-17] and a performance up to 200 Vs^{-1} has been described in the literature for OLC micro-supercapacitors (i.e., ultrathin electrodes of just a few micrometers).^[18] While there are many different synthesis methods for carbon onions, currently the only scalable synthesis route employs thermal annealing of detonation nanodiamonds above $1000 \text{ }^\circ\text{C}$, yielding a high level of control over the resulting OLC structures.^[19] The excellent power handling ability of OLC is related to the absence of intraparticle porosity and only external surface area giving rise to beneficially high ion mobility,^[20] even at very low operational temperatures below $0 \text{ }^\circ\text{C}$.^[21] However, the absence of internal particle porosity^[22] and the nanoscopic particle diameter of around 5-10 nm limits the total specific surface area to around $200\text{-}600 \text{ m}^2\text{g}^{-1}$.^[14, 16, 17] Consequently, only a moderate specific capacitance between 20 and 60 Fg^{-1} can be found in organic electrolyte which

corresponds to a low energy density of typically below 10 Whkg^{-1} .^[17] Such performance is very low compared to AC or other porous carbons, with typically more than $1200 \text{ m}^2\text{g}^{-1}$ and more than 100 Fg^{-1} .^[23] Yet, even the latter value corresponds to an energy density roughly one order of magnitude below that of lithium ion batteries which results in vast research efforts being invested in exploring facile ways to enhance the energy storage capacitive of supercapacitors.^[5, 24]

Currently, the literature shows two general approaches to increase the capacitance of carbon materials: (1) increasing the operation voltage by use of advanced electrolytes, or (2) adding redox active materials for so called pseudocapacitors. In the case of carbons with moderate or non-optimized pore structure, there exists a third approach: (3) increasing the specific surface area by chemical or physical activation. For example, physical activation in air^[22] or chemical activation with $\text{H}_2\text{SO}_4/\text{HNO}_3$ or KOH mixtures^[25] was demonstrated to increase the surface area of carbon onions to $650\text{-}820 \text{ m}^2\text{g}^{-1}$ with an capacitance of more than 120 Fg^{-1} in aqueous electrolytes. The finite ability of nanoporous carbons to screen electric charges, however, presents an upper capacitance limit to this approach^[26].

Pseudocapacitors capitalize the high energy density inherent to reversible redox reactions and provide another facile way to enhancing the energy ratings of supercapacitors. Motivated by the excellent electrical conductivity and fast ion electrosorption dynamics in carbon onion electrodes, OLC pseudocapacitors are a promising technology. In specific, three systems have been investigated: (a) adding redox active metal oxides to carbon onions,^{[27] [28]} (b) functionalization with electrochemical active polymers like polyaniline,^[29] or (c) decorating the onion surface with redox-active surface groups such as quinones.^[15] The latter provides a particularly attractive approach since simple addition of quinones to the electrolyte^[30] or by dispersion of the carbon powder in quinone containing solution can be used instead of more elaborate hydrothermal synthesis of metal oxide particles.^[15]

The redox activity and high electrochemical reversibility of quinones has been studied in the literature before.^[31]^[32] For example, Roldan et al. added hydroquinones directly to the aqueous electrolyte (1 M H₂SO₄) to increase the capacitance of an AC supercapacitor by more than 300 % (i.e., up to 900 Fg⁻¹; yet, only at very small current densities).^[33] Another synthesis procedure was described by Balach et al. via immersing porous carbon micro-particles in different types of quinone-containing solutions to reach values of ~900 Fg⁻¹ in 1 M HClO₄.^[34] Other carbon materials used in combination with quinones include carbon fabrics,^[35] graphene nanosheets,^[36] and carbon nanotubes.^[37] Recently, quinone decoration on carbon onions was explored in Ref.^[15] achieving a specific capacitance of 267 Fg⁻¹ at 5 mVs⁻¹ for a high loading of 9,10-phenanthrenequinones (PQ) in a three-electrode setup (half-cell experiment); yet, the material showed a limited power handling ability with a drop of the specific capacitance to just 50 Fg⁻¹ at 2 Vs⁻¹. The latter study also employed only small amounts of quinone-decorated onions drop casted on glassy carbon, while for the practical implementation of this material data on electrode films is needed and the performance of a full cell (two-electrode setup) is necessary. It is important to note that all aforementioned approaches were based on the conventional electrode concept of using carbon particles glued together with a polymer binder, which in turn, is adding additional resistance and dead mass to the system.

The literature documents the promising improvement of energy storage capacity via quinone-modification of carbon surfaces; yet the highest benefit for supercapacitors is only achieved when addressing both energy rating and power handling. The latter is commonly limited in AC or other materials with a large intraparticle porosity and in consequence often large amounts of conductive additive or binder were used reaching only 75 mass% of active material.^[36, 37] Specifically for carbon onions, binder-free electrodes are desirable in order to preserve the high intrinsic electrical conductivity of carbon onions which is lowered, effectively, when adding significant amounts of polymer binder. In general, the preparation

technique and specifics of carbon electrodes has a strong impact on the supercapacitor performance.^[38] Most commonly, electrodes are produced by mixing carbon powders with 5-10 mass% polytetrafluoroethylene (PTFE),^[33] while exploratory studies on the electrochemical performance of materials may rely on drop-casting of sulfonated tetrafluoroethylene based fluoropolymer-copolymer / carbon ink on glassy carbon.^[34] These methods using drop-casting on conductive substrates are suitable for electrochemical testing, but are disadvantageous for a large scale preparation, problematic to handle, and the substrate is typically not included in the capacitance or energy density calculations.

In our study, we present a new synthesis method to obtain binder-free, free-standing, and highly conductive electrodes consisting of OLC and well-established carbonized polyacrylonitrile (PAN) fibers derived from electrospinning. Electrospinning presents a facile way to obtain polymer fiber mats with a high level of control over fiber diameter and chemical composition.^[39, 40] Using further thermal treatment, polymer fibers can be carburized without losing the shape and mechanical stability; yet, the remaining large interfiber space typically remains unused. Our approach entails actually utilizing both the high connectivity of carburized PAN fibers and filling the interfiber space with carbon onions to capitalize a superior electrical conductivity and eliminate the need for polymer binder. To advance beyond merely designing an improved concept for OLC electrodes, we utilize our novel onion-like carbon / carbon fiber (OLC/CF) hybrid mats as a substrate for facile quinone-decoration.

2. Results and discussion

2.1 Morphological and structural characterization

Electrospinning of PAN fibers is a well-established and extensively investigated procedure.^[40, 41] Since (partially) graphitic carbon electrodes are needed for electrochemical applications, the as-spun PAN fibers need to undergo thermochemical treatment: first, an oxidation in air, and second, a carburization in argon. As seen from **Fig. 1A-C**, this two-step process preserves the structural integrity and the continuous, highly interconnected network of fibers of the fiber mats. The high temperature treatment in argon at 1700 °C also causes a significant reduction on fiber diameter from 264±53 nm (as-spun), and 303±84 nm (after oxidation) to 144±33 nm (carbon fiber - CF) (**Fig. 1D**) with a total fiber mat thickness of ca. 50 μm (CF) measured (*Supporting Information, Fig. S1A*).

The starting material for OLC is ND used in form of a stable dispersion in water with an average (particle) size of around 8 nm for the simplicity of introducing it later into the interfiber space of oxidized PAN fibers (**Fig. 1E**). This is in agreement with the primary particle size of around 5 nm as seen with TEM (**Fig. 1F**). The ND particles showed a diamond core with a (111)-plane lattice spacing of 0.21 nm and was covered with sp²-hybridized carbon shells, as seen from **Fig. 1F**. Like PAN, also ND particles need to be transformed to sp²-hybridized carbon prior to use in supercapacitors. This is accomplished by thermal annealing in vacuum or inert gas atmospheres. Using the same conditions as needed for the transition of oxidized PAN fibers to carbon nanofibers (i.e., 1700 °C), we obtained highly graphitic OLC particles exhibiting a highly defective fullerene-like structure with several shells (**Fig. 1G**) and a lattice spacing of 0.34 nm for the graphite (002)-plane.

We see from these TEM micrographs that annealing either nanodiamonds or oxidized PAN fibers in argon at 1700 °C yields highly graphitic carbon materials. Thus, our approach was to synergistically combine the final heat treatment process by drop-casting ND particles of a stable dispersion into the interfiber space of oxidized PAN fibers (**Fig. 2**). As seen visually

from the photograph, oxidation at 250 °C in air renders the color of white electrospun PAN fibers mats (**Fig. 2A**) to amber (**Fig. 2B**). After drop-casting of ND particles, an additional color change to dark brown occurs and finally to black after high temperature annealing (**Fig. 2C-D**). During this process, ND powders alone lose around 30 % of the initial mass due to the desorption of oxygen containing surface functional groups and carbon etching.^[22] For comparison, the mass loss of PAN alone is even more dramatic with levels around 60 % coming from the evolution of oxygen-, nitrogen-, and hydrogen- containing gases.^[42] The hybrid systems of PAN50, PAN250, and PAN500 show after thermal annealing at 1700 °C a mass loss of ca. 70 %. Interestingly, all OLC/CF hybrid mats show approximately the same mass loss although they are mostly consisting of ND which is related to enhanced carbon etching by reactive gases coming from the ND and the polyacrylonitrile. Oxygen-containing functional groups are released during annealing in argon and readily react with carbon; this results in the evolution of CO and CO₂, which lead to carbon etching per the Boudouard reaction.^[43] The thickness of the hybrid mats did not change significantly after heat treatment and we measured values between 20 and 60 μm for the different filling states (see *Supporting Information*, **Fig. S1A**).

After drop casting and drying in vacuum, the interfiber space is partially filled with ND and we find an additional ad-layer of ND particles on top of the fiber mat (**Fig. 3A,C**). The final heat treatment step at 1700 °C then transitions the oxidized PAN fibers and the infiltrated ND particles jointly to carbon fibers and carbon onions, respectively. We see a shrinkage for the fiber diameters (**Fig. 1C,D**) and in particular, cross-sectional SEM micrographs show shrunk CF fibers in channels of the former size of the original PAN fibers within a consolidated matrix of carbon onions (**Fig. 3B**). Mechanical tension during thermal annealing also causes larger pore openings in the range 1-2 μm (**Fig. 3D**).

Transmission electron micrographs further corroborate the synergistic co-transformation of oxidized PAN to CF and ND to OLC (**Fig. 3E-H**). Structurally and morphologically, OLC/CF

hybrid mats exhibit the same features as when synthesized CF or OLC separately (cf. **Fig. 1**). Both carbon fibers and carbon onions show a high degree of structural ordering, characteristic for both materials synthesized at elevated temperature of 1700 °C.^[42] Yet, the loading with onions is not just filling of the free interfiber space, but is also interconnected via local sintering of the OLC (**Fig. 3F**) as shown in a recent study.^[22]

The partially graphitic state of OLC and CF, and also OLC/CF hybrid fiber mats, is shown by the presence of characteristic D- and G-modes between 1200 and 1700 cm⁻¹ and a distinct range of overtones and combinational modes between 2300 and 3400 cm⁻¹ (**Fig. 4A**). The G-mode between 1580 and 1600 cm⁻¹ is a first-order peak with E_{2g}-symmetry and representative for sp²-hybridized carbon.^[44] The D-mode between 1340 and 1345 cm⁻¹ relates to defects and disorder induced phonon transitions.^[45] The I_D/I_G-ratio of carburized PAN and carbon onions is 1.36±0.02 and 1.24±0.03, as typical for a high degree of carbon ordering. This result is supported by presence of sharp D- and G-peaks with a rather narrow full-width at half maximum of 40-70 cm⁻¹ (**Fig. 4B**).^[44] By adding quinones to the composite electrode (PQ-max) via drop casting followed by extensive washing the Raman signal of PQ is still visible in the composite, indicating the stable adsorption and high degree of functionalization (**Fig. 4A**). As expected for a high degree of graphitization, we also observe a high electrical conductivity as measured with a four-point-probe (**Fig. 4C**). OLC powders, after compressing to free-standing pellets, show conductivities between 0.9 and 1.8 Scm⁻¹, whereas PTFE-bound OLC electrodes show values of 0.5-1.1 Scm⁻¹ in excellent agreement with the literature.^[14, 17] For comparison, the electrical conductivity of film electrodes of pure carbon black with 10 mass% PTFE and activated carbon with 5 mass% PTFE are ~2 and ~0.1 Scm⁻¹, respectively.^[46] Although the degree of carbon ordering for CF and OLC is very similar based on our Raman investigation, we see that CF fiber mats have an order of magnitude higher conductivity (~26 Scm⁻¹). Even higher values are obtained for OLC/CF hybrid mats with a maximum of ~54 Scm⁻¹ for CF500 and it is important to note that this value is not reduced when adding PQ

to the latter (**Fig. 4C**). These findings exemplify that the conductivity of the composite electrode is very sensitive to particle-particle resistance and the high conductivities of CF and OLC/CF hybrid mats are afforded by the high interconnectivity and the continuous network of fused carbon material.

The specific surface area of carbon onions, typically in the range of 200-600 m²g⁻¹,^[22] represents the large external surface and does not stem from internal porosity. In this study, the surface area of carbon onions synthesized at 1700 °C is 387 m²g⁻¹ (BET) and 353 m²g⁻¹ (DFT) in agreement with literature.^[17, 22, 47] The carbonized PAN fibers show a surface area of less than 50 m²g⁻¹, which prohibits their use for supercapacitors (at least without additional physical or chemical activation). With increasing amount of carbon onions in the hybrid mat electrode, the surface area continuously increases for CF500 up to a maximum value of 313 m²g⁻¹ (BET) and 291 m²g⁻¹ (DFT). This value is still slightly smaller than the surface area of loose OLC powder because of the sintering of carbon onions to other carbon onions and superficial fusing to CF. This is accomplished by carbon redistribution related to reactive gases coming from the ND precursor, ultimately giving rise to the formation of larger graphitic particles as shown in a recent study (cf. *Supporting Information, Fig. S2*).^[22]

2.2 Electrochemical characterization

Electrochemical testing has been performed on PTFE-bound OLC electrodes and free-standing CF and OLC/CF hybrid mats in 1 M TEA-BF₄ in acetonitrile, ACN. Cyclic voltammograms, CV, at different scan rates in a half-cell were used to demonstrate the electrochemical performance at 10 mVs⁻¹ (**Fig. 5A**) and 2 Vs⁻¹ (**Fig. 5B**). In the case of the latter high scan rate, the rectangular CV shape of the CF and OLC/CF hybrid mats is still present, whereas the CV curve for the PTFE-bound electrode indicates a significantly resistive behavior (**Fig. 5B**). We also note a pronounced butterfly-shape of CVs of all samples as a result to the non-constant differential capacitance.^[47, 48] In detail, applying a higher potential

introduces additional states, reduces the electrical conductivity of the carbon, and improves the ability to screen ionic charges. This phenomenon is known as electrochemical doping and has been described in the literature for graphite, activated carbons, carbon nanotubes, and carbon onions.^[48, 49]

Dependent on the OLC amount, the capacitance increases from below 1 Fg^{-1} to a maximum of 19.5 Fg^{-1} (CF500) at 1 V. The increase in capacitance with the amount of OLC stems from the much higher SSA of CF500 ($313 \text{ m}^2\text{g}^{-1}$ BET SSA) compared to the carbonized PAN fibers ($36 \text{ m}^2\text{g}^{-1}$ BET SSA). The PTFE-bound electrode has a slightly larger capacitance of 20.5 Fg^{-1} , because of the larger surface area; yet we see that this initially higher capacitance is readily lost at higher scan rates with a cross-over to CF500 at around 100 mVs^{-1} (**Fig. 5C**). Yet, CF500 loses just ~15% of its initial low-scan-rate capacitance, while the PTFE-bound OLC electrode shows a reduced specific capacitance of ~60 % at 2 Vs^{-1} (**Fig. 5C**). An overview of the measured electrode capacitances is given in **Table 1**.

The observations made for cyclic voltammograms of half-cell operation are confirmed for full-cell experiments (**Fig. 5D**). Direct comparison of PTFE-bound OLC electrode performance with CF500 shows that the latter exhibits a significantly higher rate handling ability when cycling up to 2.5 V cell voltage (**Fig. 5D**). When employing galvanostatic charge/discharge testing, we see that CF500 and PTFE-bound OLC electrodes show a comparable performance up to ca. 1 Ag^{-1} . With increasing the current density up to 50 Ag^{-1} the relative capacitance is as low as ~25 % for the PTFE-bound OLC electrode but still more than 70 % for the OLC/CF hybrid mat. Even for a current density of 100 Ag^{-1} the composite electrode shows a relative capacitance of more than 60 % of the low-current-density value. Thus, at higher current densities, CF500 shows superior capacitive performance and this performance remains highly stable (**Fig. 5F**). In particular, we tested the cycling stability over 10,000 cycles at 200 mVs^{-1} and for 100 h holding time at 2.5 V without any degradation, especially for the CF500.

Yet, it is clear that with such low specific capacitance, even CF500 or PTFE-bound OLC electrodes have a very limited potential as electrode material for carbon supercapacitors. Thus, we used our well-characterized OLC/CF hybrid mats as a substrate for modification with PQ. Electrochemical characterization in aqueous 1 M H₂SO₄ using CF500 with different loadings of PQ, the PTFE-bound electrode with PQ, as well as the carburized PAN electrode with PQ is presented in **Fig. 6**. Cyclic voltammetry from 0 V to -0.4 V vs. Pt of the CF500 composite electrode shows a rectangular shape with a capacitance of 34 Fg⁻¹ (**Fig. 6A**), 70 % higher than in organic electrolyte (**Fig. 5A**). With adding and increasing loading of PQ, quinone redox peaks between -0.15 V and -0.25 V vs. Pt appear and grow in intensity and area (**Fig. 6A**).

Inferred from literature, the drop-casted quinone molecules arrange parallel to the carbon onion surface, most probably due to π - π interactions.^[50] The mechanism of the proton-coupled electron transfer reaction ($2e^- / 2H^+$) between the surface bound quinones and electrolyte is described elsewhere.^[32, 51] With the maximum loading of CF500 with PQ (PQ-max), a capacitance of 288 Fg⁻¹ is measured with a maximum energy density of ~6.4 Whkg⁻¹ and a maximum power density of ~19.2 kWkg⁻¹. For comparison, using the same synthesis and experimental conditions, the PTFE-bound OLC electrode (OLC-PQ-max) and the carbon fiber electrode (CF-PQ-max) have lower capacitances of 221 Fg⁻¹ and 21 Fg⁻¹, respectively, with a maximum energy density of ~4.9 Whkg⁻¹ and a maximum power density of ~4.3 kWkg⁻¹ for OLC-PQ-max. Commercial activated carbon electrodes present much lower values with 115 Fg⁻¹ capacitance, ~2.5 Whkg⁻¹ energy density, and ~1.8 kWkg⁻¹ power density (**Fig. 6A** and **Fig. S3B**). All capacitance and capacity values are presented in **Table 1**. **Fig. 6B** also shows the performance of conventional activated carbon in form of a PTFE-bound electrode; as expected, the capacitive performance of an AC electrode drops rapidly when transitioning beyond ca. 100 mVs⁻¹ scan rate. Up to a scan rate of 200 mVs⁻¹, our data is in excellent agreement with our previous study (Ref. ^[15]) on drop-casted quinone-decorated onions on glassy carbon. For higher scan rates, for example 2 Vs⁻¹, our OLC/CF hybrid mats have the

twice the capacitance in spite of smaller surface area and lower synthesis temperature (here: 1700 °C, Anjos et al.: 1800 °C) ^[15].

These findings are supported by the electrochemical characterization in organic electrolyte. As shown before (**Fig. 5**), using 1 M TEA-BF₄ in ACN the PTFE-bound OLC electrode exhibited a lower rate handling with only ~40 % initial capacitance at 2 Vs⁻¹ scan rate (half-cell) and ~25 % at 50 Ag⁻¹ (full cell) compared to ~75 %, and ~70 % for CF500. The same result was observed in 1 M H₂SO₄ with an enormous high capacitance of more than 100 Fg⁻¹ for the PQ-loaded composite (PQ-max), only ~25 Fg⁻¹ for the PTFE-bound electrode, and ~3 Fg⁻¹ for a standard activated carbon electrode at 2 Vs⁻¹ scan rate. Even without PQ loading, the OLC/CF hybrid mats (CF500) show higher values (~35 Fg⁻¹) than the PTFE-bound OLC electrode, and activated carbon (**Fig. 6B**). These findings are additionally supported by impedance spectroscopy (**Fig. S3A**), where a clear reduction in EDR can be seen for composite electrodes as compared to PTFE bound OLC electrodes.

Electrochemical long-time stability was measured using cyclic voltammetry from 0 V to -0.4 V vs. Pt for 10,000 cycles (**Fig. 6C**). The activated carbon electrolyte as well as the CF500 composite electrode demonstrate a high stability after 10,000 cycles. After PQ-loading of the composite electrode (PQ-max) the capacitance decrease for ~10 % after 10,000 cycles, similar to previous reported literature values of 6 % ^[15]. The maximum potential window is limited to 1 V as shown in **Fig. 6D**. Using a full cell arrangement for both the CF500 electrode as well as the high-loading PQ-max electrodes shows similar data compared to the half cell experiments. By successively opening the potential window in 0.1 V steps up to -0.5 V and 0.5 V, electrode degeneration starts. This is indicated by the higher slope of CF500 using 1 V cell voltage and the appearance of additional peaks for PQ-max.

3. Conclusions

A new electrode synthesis method was developed using a carbon fiber network filled with carbon onions. For the first time, carbon onion electrodes were free-standing and binder-free with a superior rate handling in organic as well as aqueous electrolyte compared to standard PTFE-bound or drop casted carbon onions. The filling of the interfiber spacing of carbon fiber networks presents a facile way to synergistically combine the high conductivity of a continuous fiber network with the higher surface area of carbon nanoparticles (i.e., carbon onions). This method may also work as platform to prepare electrodes with other carbon or hybrid nanoparticles. The high conductivity combined with a moderate surface area also is a suitable platform for the effective functionalization with pseudocapacitive materials like quinones. The maximum decoration of the composite electrode with quinones increases the capacitance of more than 8-times to 288 Fg^{-1} in $1 \text{ M H}_2\text{SO}_4$. The electrode demonstrates a stable performance for 10,000 cycles and a fast response, resulting in more than 100 Fg^{-1} at 2 Vs^{-1} scan rate.

4. Experimental Section

Synthesis of carbon fiber, carbon onion, and composite electrodes

Carbon fiber mats were synthesized using thermal annealing of electrospun polymer fibers of polyacrylonitrile (PAN, Sigma Aldrich). For electrospinning, the polymer powder was dissolved in dimethylformamide (DMF, Sigma Aldrich, anhydrous 99.8 %) in an 8 mass% solution resulting in a viscous liquid. A 5 mL aliquot of the polymer solution was spun with a MECC electrospinning system (MECC Co.) at 15 kV using a feed rate of 0.4 mLh^{-1} and 250 mm fly distance for 10 h while using a transverse speed of 20 mms^{-1} over a travel distance of 250 mm. The electrospinning setup consisted of a syringe and a needle connected via PTFE tubing and a plate collector coated with conventional alumina foil as the substrate. After electrospinning, polymer fiber mats were converted to carbon fibers using a two-step

treatment. First, the polymer fibers were oxidized in air in a furnace at 250 °C for 30 min using a heating rate of 5 °Cmin⁻¹. To avoid large temperature variations and a deformation of the mats during heating, the samples were placed between two graphite plates. In the second step, the oxidized PAN fiber mats were thermally annealed in a water cooled high temperature furnace with tungsten heater (Thermal Technology Inc.) in pure argon (purity 4.6). The used temperature profile exhibited three holding temperatures of 700 °C and 1100 °C for 1 h, and 1700 °C for 3 h. The heating rate was 5 °Cmin⁻¹ and the cooling rate 15 °Cmin⁻¹.

Composite electrodes consisting of carbon fibers and carbon onions were made using a two-step approach: drop casting of nanodiamonds into polymer fiber mats followed by a thermal annealing process to synergistically convert the composite to conductive carbon fibers and carbon onions. The nanodiamonds were supplied in a 5 mass% dispersion in water (Single-digit nanodiamonds 5 mass% in water, PlasmaChem) and the supplier used a post-synthesis treatment to produce a dispersion composed of so-called single-digit nanodiamonds fully dispersed and de-agglomerated in water with an average aggregate size of 5-15 nm and a specific surface area of 350-390 m²g⁻¹. The dispersion was drop-casted in several steps on the oxidized PAN polymer fiber mats until the desired mass loading had been reached. Between the casting steps, the fiber mats were dried in a vacuum furnace at 120 °C for 1 h at 10 mbar to evaporate the solvent (H₂O). The filling degrees with nanodiamonds were 50, 250, or 500 mass% (related to the mass of oxidized polymer fibers). The samples are referred to as PAN50, PAN250, or PAN500, respectively. After the implementing nanodiamonds in the interfiber space, the same thermal annealing process as already mentioned for the electrospun PAN fibers was used to create free-standing and binder-free carbon fiber electrodes filled with onion-like carbon (CF - CF500).

For comparison, conventional PTFE-bound electrodes were prepared with carbon onions synthesized with the same temperature treatment protocol as outlined before. Free-standing carbon onion electrodes were prepared by mixing 90 mass% of carbon onions with 10 mass%

polytetrafluoroethylene (60 mass% PTFE in water, Sigma Aldrich) together with ethanol to make a slurry. For the activated carbon electrode, 95 mass% of carbon and 5 mass% PTFE were used. The slurries were tip sonicated for 10 min at ~4 W, then constantly stirred until a dough-like mass was developed. Using a twin roller (MTI HR01, MTI Corporation) the PTFE-bound mass was rolled to free-standing sheets with a thickness of ~100 μm . Prior to use, the electrodes were dried at 120 $^{\circ}\text{C}$ in vacuum at 2 kPa for 24 h. For half-cell experiments, the oversized counter electrode was composed of activated carbon (YP80, Kuraray Chemical Co.) and 5 mass% PTFE with a thickness of ~300 μm . After drying, the working electrodes were prepared by punching out 6 mm disks of carbon fiber mats, OLC/CF hybrid fiber mats, and PTFE-bound carbon onion and activated carbon electrodes.

Decoration of composite electrodes with 9,10-phenanthrenequinones

The CF500 hybrid fiber mats were functionalized with 9,10-phenanthrenequinones (PQ). First, the PQ powder (Sigma Aldrich) was dissolved in Ethanol (1.1 mg mL^{-1}) and filtered several times with a syringe filter (0.1 μm pore size). The resulting solution was drop-casted using a volume of 20 μL on the electrodes, dried at room temperature, and this process was repeated several times to prepare two different levels of PQ loading. For the sample PQ-20 only one casting step was used, resulting in an overall volume of 20 μL . For sample PQ-200, 10 casting steps with an overall volume of 200 μL PQ-solution were used. To prepare a composite electrode with the maximum loading of PQ (PQ-max), the electrode was put into the solution with volume of 5 mL for 24 h. For comparison, the PTFE-bound carbon onion electrode (OLC-PQ-max) as well as the CF fiber electrode (CF-PQ-max) were also soaked in the 5 mL solution for 24 h. After decoration with PQ, all samples were rinsed with ethanol for several times and dried at room temperature in vacuum at 2 kPa for 24 h. This step was adopted in order to remove PQ not adsorbed on the electrode's surface to avoid the addition of (electrochemically) dead mass.

Structural characterization

Electron microscopy

Scanning electron microscope (SEM) images were taken with a FEI Versa 3D Dual Beam (FEI) at 10 kV. Free-standing electrodes as well as OLC powders were mounted on a steel sample holder with sticky carbon tape. For cross sectional images, the samples were cut with a razor blade and fixed with carbon tape on a 90° tilted sample holder. Samples consisting of polymer or nanodiamond were sputter coated prior to the imaging with gold for 60 s with an Autofine Coater (JEOL). The fiber diameter distribution was derived from SEM images using ImageJ. For each sample, two different batches were prepared and the diameters were manually read out on five different positions on the sample. The total number of measured diameters was 50 and a Gaussian function was used to fit the data.

Samples for transmission electron microscopy (TEM) were prepared by dispersing powders or fibers in ethanol and drop casting them on a copper grid with a lacey carbon film (Gatan). All measurements were carried out with a JEOL 2100F operating at 200 kV. Carbon fiber mats or composite mats were first tip sonicated in ethanol for 5 min to make a drop casting on the copper grids possible.

Raman spectroscopy

Raman spectra were measured with a Renishaw inVia Raman Microscope using an Nd-YAG laser with an excitation wavelength of 532 nm. The grating was 2400 lines mm⁻¹ yielding a spectral resolution of ~1.2 cm⁻¹ and the spot size on the sample was in the focal plane ~2 μm with an output power of 0.2 mW. Spectra were recorded for 20 s and accumulated 50-times to

obtain a high signal-to noise and signal-to-background ratio. Peak fitting was performed by employing two Lorentzian peaks, one for the D- and the other for the G-mode.

Conductivity measurements via four-point probe

The conductivity of the electrodes was determined with a custom built 4-point probe (tip diameter: 1.5 mm; tip distance 1.75 mm). The areal resistance was measured 10 times on different positions of the electrode material (3x3 cm²) and equation (1) was used to calculate the electrode conductivity normalized to the thickness.^[52]

$$\sigma = \frac{\ln(2)}{\pi} \frac{I}{U \cdot d} \quad (1)$$

In this equation, I is the current, U the voltage, and d the thickness of the electrode measured with a micrometer screw.

Gas sorption analysis

To remove adsorbed molecules from the surface, all samples were degassed at 200 °C for 30 min and subsequently at 300 °C for 20 h at a relative pressure of 0.1 Pa. Nitrogen gas sorption analysis at -196 °C was performed with a Quantachrome Autosorb 6B system. The pore size distribution (PSD) was derived using the quenched-solid density functional theory (QSDFT) supplied by Quantachrome assuming a slit shape pore model.^[53] The specific surface area (SSA) using the BET-equation was calculated in the linear regime of the measured isotherms at a partial pressure range between 0.1 and 0.3 P/P₀.^[54]

Particle size analysis

Particle size analysis was performed using centrifugal sedimentation analysis (LUMiSizer; LUM Corporation, USA). The nanodiamond powder was dispersed in water (0.5 mass%) via tip sonication at ~4 W for 1 h, and tested in a range from 200-4000 rpm.

Electrochemical characterization

1 M tetraethylammonium tetrafluoroborate (TEA-BF₄) in acetonitrile (ACN) from BASF and 1 M sodium sulfate (H₂SO₄) from Sigma Aldrich were used as electrolytes. We used a two-electrode as well as three-electrode setup in this study to provide, for the first time, comparative half- and full-cell performance data. The prepared electrodes (6 mm in diameter) were separated by a glass-fiber separator with a diameter of 13 mm (type GF/D, Whatman). Using 1 M TEA-BF₄ in ACN the electrode / separator / electrode arrangement was placed between two carbon-coated aluminum foils (diameter 12 mm, type Zflo 2653, Exopack technologies) and compressed with spring-loaded titanium pistons. For the aqueous system, in this case using 1 M H₂SO₄, the electrode / separator / electrode sandwich was placed between platinum disks as current collectors (12 mm in diameter and 100 μm thick, Mateck) and compressed with spring-loaded polyether ether ketone (PEEK) pistons. In the three-electrode setup, the counter electrode consisted of activated carbon (YP80, Kuraray) with 5 mass% PTFE and a thickness of 300 μm. The reference electrode in the organic system was activated carbon (YP50, Kuraray) with 5 mass% PTFE and in the aqueous system a platinum wire (Carl Schaefer) with a diameter of 0.5 mm. The cells for organic electrolyte were dried at 120 °C and a vacuum of 2 kPa for 12 h before they were put in an argon-filled glove box (MBraun Labmaster 130; O₂, H₂O < 1 ppm), where they were vacuum filled with a syringe containing 1 M TEA-BF₄ in ACN. The cells for the aqueous system were directly, without further drying, vacuum filled with a syringe and the mentioned electrolyte.

All electrochemical measurements were carried out using a VSP300 or VMP300 potentiostat/galvanostat from Bio-Logic in cyclic voltammetry (CV) and galvanostatic mode (GCPL). In the organic system cyclic voltammograms at different scan rates from 1 mVs⁻¹ to 2 Vs⁻¹ from -1 V to +1 V vs. AC were conducted in a half cell.^[47, 55] Each voltage was applied for 3-times and the capacitance at 1 V for every scan rate was calculated using equation (2).
[56]

$$C = \frac{\int_{t_0}^{t_{end}} I(t) dt}{U} \quad (2)$$

with the capacitance C, the time t (t₀: start of discharge, t_{end}: end of discharge), and the potential U. The specific capacitance in the three electrode setup was determined with equation (3).^[57, 58]

$$C_{sp} = \frac{C}{m} \quad (3)$$

with the mass m of the working electrode. Using GCPL mode in a full cell arrangement (two electrodes) the current was varied to apply different current densities from 0.1 Ag⁻¹ to 100 Ag⁻¹ with 10 s resting time between charging/discharging and a potential limitation of 2.5 V. For PTFE-bound electrodes the maximum current density was 50 Ag⁻¹ due to current limitations of the potentiostat. The specific current relates in this case to the mass of both electrodes and the resulting capacitance was calculated from the current and the time for discharge with respect to the IR drop of the cell. Stability was measured using both, long-time voltage floating tests and voltammetric cycling. The long-time voltage floating test in a full cell was performed between 0 V and 2.5 V with a constant current of 0.5 Ag⁻¹ and a holding time of 10 h. After galvanostatic cycling for 3-times, the voltage was held for 10 h at 2.5 V and procedure was repeated to an overall holding time of 100 h. Voltammetric cycling from 0 to 2.5 V at 200 mVs⁻¹ was repeated for 10,000-times and every 200 cycles were recorded.

In the aqueous system only cyclic voltammetry was used for electrochemical characterization. Using a three electrode set up, different scan rates over a range of 3 orders of magnitude from 1 mVs^{-1} to 2 Vs^{-1} were applied from 0 to -0.4 V . In the two-electrode configuration, the potential window was successively opened from -0.2 V to $+0.2 \text{ V}$ in 100 mV steps to the maximal potential window of -0.5 V and $+0.5 \text{ V}$. Electrochemical stability was tested using cyclic voltammetry from 0 V to -0.4 V vs. Pt at 200 mV/s scan rate for 10,000 cycles. The capacitance in the aqueous system was calculated using equation (4).^[58, 59]

$$C = \frac{\int_{U_o}^{U_{end}} \frac{IdU}{v}}{m\Delta U} \quad (4)$$

with the current I , the scan rate v , the mass of the working electrode m , and the potential window ΔU . The capacity of one electrode was measured according to equation (5).^[58, 59]

$$C = \frac{\int_{U_o}^{U_{end}} \frac{IdU}{v}}{m} \quad (5)$$

with the current I , the scan rate v , and the mass of the working electrode m .

Electrochemical impedance spectroscopy was performed at 0 V in full cells for the CF 500, PQ-max and OLC-PQ-max system in the frequency range from 100 kHz to 10 mHz with 6 points per decade and 5 repetitions per point. The excitation amplitude was 5 mV .

Supporting Information

Supporting Information is available from the Wiley Online Library or from the author.

Acknowledgements

The INM (www.inm-gmbh.de) is part of the Leibniz Research Alliance Energy Transition (LVE). We acknowledge funding from the German Federal Ministry for Research and Education (BMBF) in support of the nanoEES^{3D} project (award number 03EK3013) as part of the strategic funding initiative energy storage framework. We kindly acknowledge additional funding via the INM FOCUS project ELECTRIC and thank Prof. Eduard Arzt (INM) for his continuing support.

Received: ((will be filled in by the editorial staff))
Revised: ((will be filled in by the editorial staff))
Published online: ((will be filled in by the editorial staff))

- [1] F. Béguin, V. Presser, A. Balducci, E. Frackowiak, *Advanced Materials* 2014, 26, 2219.
- [2] Z. Yang, J. Zhang, M. C. Kintner-Meyer, X. Lu, D. Choi, J. P. Lemmon, J. Liu, *Chem Rev* 2011, 111, 3577.
- [3] J. B. Goodenough, *Energ Environ Sci* 2014, 7, 14; J. N. Tiwari, R. N. Tiwari, K. S. Kim, *Progress in Materials Science* 2012, 57, 724.
- [4] N. S. Choi, Z. Chen, S. A. Freunberger, X. Ji, Y. K. Sun, K. Amine, G. Yushin, L. F. Nazar, J. Cho, P. G. Bruce, *Angewandte Chemie International Edition* 2012, 51, 9994; C. Liu, F. Li, L. P. Ma, H. M. Cheng, *Advanced Materials* 2010, 22, E28.
- [5] P. Simon, Y. Gogotsi, B. Dunn, *Science Magazine* 2014, 343.
- [6] H. Shi, *Electrochimica Acta* 1996, 41, 1633; D. Qu, H. Shi, *Journal of Power Sources* 1998, 74, 99.
- [7] K. H. An, W. S. Kim, Y. S. Park, J.-M. Moon, D. J. Bae, S. C. Lim, Y. S. Lee, Y. H. Lee, *Advanced Functional Materials* 2001, 11, 387.
- [8] L. L. Zhang, R. Zhou, X. Zhao, *Journal of Materials Chemistry* 2010, 20, 5983.
- [9] V. Presser, L. Zhang, J. J. Niu, J. McDonough, C. Perez, H. Fong, Y. Gogotsi, *Advanced Energy Materials* 2011, 1, 423.
- [10] A. Fuertes, G. Lota, T. Centeno, E. Frackowiak, *Electrochimica Acta* 2005, 50, 2799.
- [11] M. Toupin, D. Bélanger, I. R. Hill, D. Quinn, *Journal of power sources* 2005, 140, 203.
- [12] Y. Gogotsi, V. Presser, *Carbon nanomaterials*, CRC Press, 2013; M. E. Plonska-Brzezinska, L. Echegoyen, *Journal of Materials Chemistry A* 2013, 1, 13703.
- [13] H. W. Kroto, J. R. Heath, S. C. O'Brien, R. F. Curl, R. E. Smalley, *Nature* 1985, 318, 162; I. Suarez-Martinez, N. Grobert, C. P. Ewels, *Carbon* 2012, 50, 741.
- [14] C. Portet, G. Yushin, Y. Gogotsi, *Carbon* 2007, 45, 2511.
- [15] D. M. Anjos, J. K. McDonough, E. Perre, G. M. Brown, S. H. Overbury, Y. Gogotsi, V. Presser, *Nano Energy* 2013, 2, 702.
- [16] D. Pech, M. Brunet, H. Durou, P. Huang, V. Mochalin, Y. Gogotsi, P.-L. Taberna, P. Simon, *Nature Nanotechnology* 2010, 5, 651.
- [17] J. K. McDonough, A. I. Frolov, V. Presser, J. Niu, C. H. Miller, T. Ubieto, M. V. Fedorov, Y. Gogotsi, *Carbon* 2012, 50, 3298.
- [18] P. Huang, M. Heon, D. Pech, M. Brunet, P.-L. Taberna, Y. Gogotsi, S. Lofland, J. D. Hettinger, P. Simon, *Journal of Power Sources* 2013, 225, 240.
- [19] Y. V. Butenko, V. L. Kuznetsov, A. L. Chuvilin, V. N. Kolomiichuk, S. V. Stankus, R. A. Khairulin, B. Segall, *Journal of Applied Physics* 2000, 88, 4380; V. L. Kuznetsov, A. L. Chuvilin, Y. V. Butenko, I. Y. Mal'kov, V. M. Titov, *Chemical Physics Letters* 1994, 222, 343; S. Tomita, A. Burian, J. C. Dore, D. LeBolloch, M. Fujii, S. Hayashi, *Carbon* 2002, 40, 1469.
- [20] K. L. Van Aken, J. K. McDonough, S. Li, G. Feng, S. M. Chathoth, E. Mamontov, P. F. Fulvio, P. T. Cummings, S. Dai, Y. Gogotsi, *Journal of Physics: Condensed Matter* 2014, 26, 284104.
- [21] R. Lin, P.-L. Taberna, S. Fantini, V. Presser, C. R. Pérez, F. Malbosc, N. L. Rupesinghe, K. B. Teo, Y. Gogotsi, P. Simon, *The Journal of Physical Chemistry Letters* 2011, 2, 2396.
- [22] M. Zeiger, N. Jäckel, M. Aslan, D. Weingarth, V. Presser, *Carbon* 2015, 84, 584.
- [23] W. Gu, G. Yushin, *Wiley Interdisciplinary Reviews: Energy and Environment* 2014, 3, 424.
- [24] J. R. Miller, A. F. Burke, *The Electrochemical Society Interface* 2008, 17, 53.
- [25] W. Gu, N. Peters, G. Yushin, *Carbon* 2013, 53, 292; Y. Gao, Y. S. Zhou, M. Qian, X. N. He, J. Redepenning, P. Goodman, H. M. Li, L. Jiang, Y. F. Lu, *Carbon* 2013, 51, 52.
- [26] O. Barbieri, M. Hahn, A. Herzog, R. Kötz, *Carbon* 2005, 43, 1303.

- [27] Y. Wang, S. F. Yu, C. Y. Sun, T. J. Zhu, H. Y. Yang, *Journal of Materials Chemistry* 2012, 22, 17584.
- [28] M. V. K. Azhagan, M. V. Vaishampayan, M. V. Shelke, *Journal of Materials Chemistry A* 2014, 2, 2152.
- [29] I. Kovalenko, D. G. Bucknall, G. Yushin, *Advanced Functional Materials* 2010, 20, 3979.
- [30] E. Frackowiak, M. Meller, J. Menzel, D. Gastol, K. Fic, *Faraday discussions* 2014, 172, 179.
- [31] E. Laviron, *Journal of Electroanalytical Chemistry and Interfacial Electrochemistry* 1984, 164, 213.
- [32] S. Bailey, I. Ritchie, *Electrochimica acta* 1985, 30, 3.
- [33] S. Roldán, M. Granda, R. Menendez, R. Santamaria, C. Blanco, *The Journal of Physical Chemistry C* 2011, 115, 17606
- [34] J. Balach, M. M. Bruno, N. G. Cotella, D. F. Acevedo, C. A. Barbero, *Journal of Power Sources* 2012, 199, 386.
- [35] K. Kalinathan, D. P. DesRoches, X. Liu, P. G. Pickup, *Journal of Power Sources* 2008, 181, 182.
- [36] H. Wang, H. Wu, Y. Chang, Y. Chen, Z. Hu, *Chinese Sci Bull* 2011, 56, 2092.
- [37] X. Chen, H. Wang, H. Yi, X. Wang, X. Yan, Z. Guo, *The Journal of Physical Chemistry C* 2014, 118, 8262.
- [38] V. Ruiz, C. Blanco, M. Granda, R. Menéndez, R. Santamaría, *Journal of applied electrochemistry* 2007, 37, 717.
- [39] X. Wang, B. Ding, G. Sun, M. Wang, J. Yu, *Progress in Materials Science* 2013, 58, 1173; Z.-M. Huang, Y.-Z. Zhang, M. Kotaki, S. Ramakrishna, *Composites science and technology* 2003, 63, 2223.
- [40] L. Zhang, A. Aboagye, A. Kelkar, C. Lai, H. Fong, *Journal of Materials Science* 2014, 49, 463.
- [41] T. Wang, S. Kumar, *Journal of Applied Polymer Science* 2006, 102, 1023.
- [42] M. S. A. Rahaman, A. F. Ismail, A. Mustafa, *Polymer Degradation and Stability* 2007, 92, 1421.
- [43] V. Kuznetsov, Y. V. Butenko, V. Zaikovskii, A. Chuvilin, *Carbon* 2004, 42, 1057.
- [44] A. C. Ferrari, *Solid State Communications* 2007, 143, 47.
- [45] F. Tuinstra, *The Journal of Chemical Physics* 1970, 53, 1126; M. A. Pimenta, G. Dresselhaus, M. S. Dresselhaus, L. G. Cancado, A. Jorio, R. Saito, *Physical Chemistry Chemical Physics* 2007, 9, 1276.
- [46] N. Jäckel, D. Weingarth, M. Zeiger, M. Aslan, I. Grobelsek, V. Presser, *Journal of Power Sources* 2014, 272, 1122.
- [47] D. Weingarth, M. Zeiger, N. Jäckel, M. Aslan, G. Feng, V. Presser, *Advanced Energy Materials* 2014, 4, 1400316.
- [48] H. Gerischer, R. McIntyre, D. Scherson, W. Storck, *Journal of Physical Chemistry* 1987, 91, 1930.
- [49] A. Kornyshev, N. Luque, W. Schmickler, *Journal of Solid State Electrochemistry* 2014, 18, 1345; P. Ruch, L. Hardwick, M. Hahn, A. Foelske, R. Kötz, A. Wokaun, *Carbon* 2009, 47, 38.
- [50] D. M. Anjos, A. I. Kolesnikov, Z. Wu, Y. Cai, M. Neurock, G. M. Brown, S. H. Overbury, *Carbon* 2013, 52, 150.
- [51] K. Kano, B. Uno, *Analytical Chemistry* 1993, 65, 1088.
- [52] F. M. Smits, *Bell System Technical Journal* 1958, 37, 711.
- [53] G. Y. Gor, M. Thommes, K. A. Cychoz, A. V. Neimark, *Carbon* 2012, 50, 1583; A. V. Neimark, Y. Lin, P. I. Ravikovitch, M. Thommes, *Carbon* 2009, 47, 1617.

- [54] S. Brunauer, P. H. Emmett, E. Teller, *Journal of the American Chemical Society* 1938, 60, 309.
- [55] P. W. Ruch, D. Cericola, M. Hahn, R. Kötz, A. Wokaun, *Journal of Electroanalytical Chemistry* 2009, 636, 128.
- [56] B. E. Conway, *Electrochemical Supercapacitors*, Springer, Berlin 1999.
- [57] M. D. Stoller, R. S. Ruoff, *Energ Environ Sci* 2010, 3, 1294; F. Beguin, E. Frackowiak, *Supercapacitors*, Wiley, Weinheim 2013.
- [58] D. M. Anjos, J. K. McDonough, E. Perre, G. M. Brown, S. H. Overbury, Y. Gogotsi, V. Presser, *Nano Energy* 2013, 2, 702
- [59] S. Zhang, N. Pan, *Advanced Energy Materials* 2015, 5.
- [60] A. Le Comte, D. Chhin, A. Gagnon, R. Retoux, T. Brousse, D. Belanger, *Journal of Materials Chemistry A* 2015.

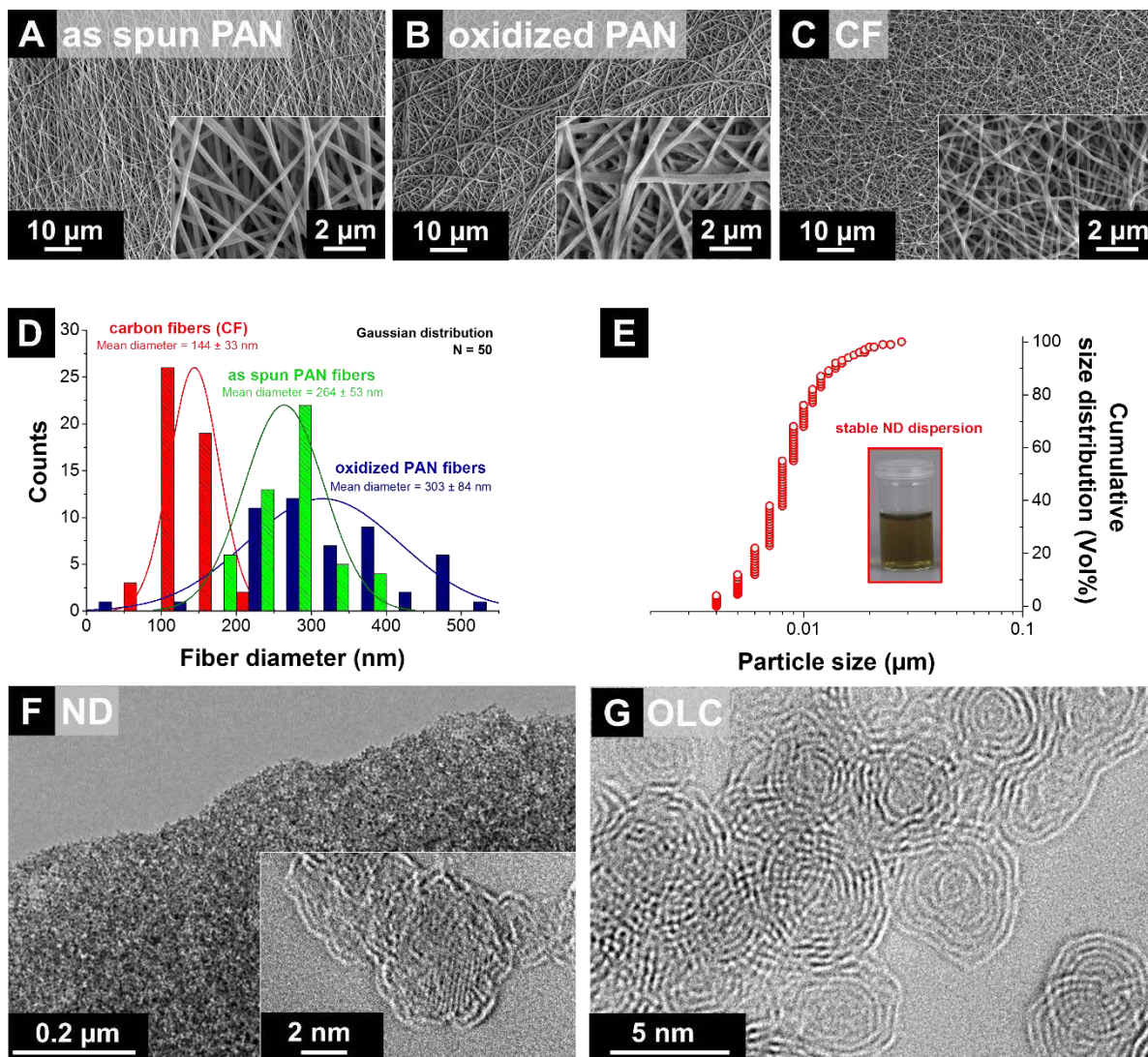


Figure 1. Scanning electron micrographs of as spun PAN fibers (A), of oxidized PAN fibers (B), of carbon fibers annealed at 1700 °C in argon (C), and transmission electron micrographs of nanodiamonds (F) and carbon onions (G). The fiber diameter distribution for the three synthesis steps (as spun, oxidized, carburized) is shown in (D). Centrifugal sedimentation analysis of a stable nanodiamond dispersion measured in a 0.5 mass% water dispersion (E).

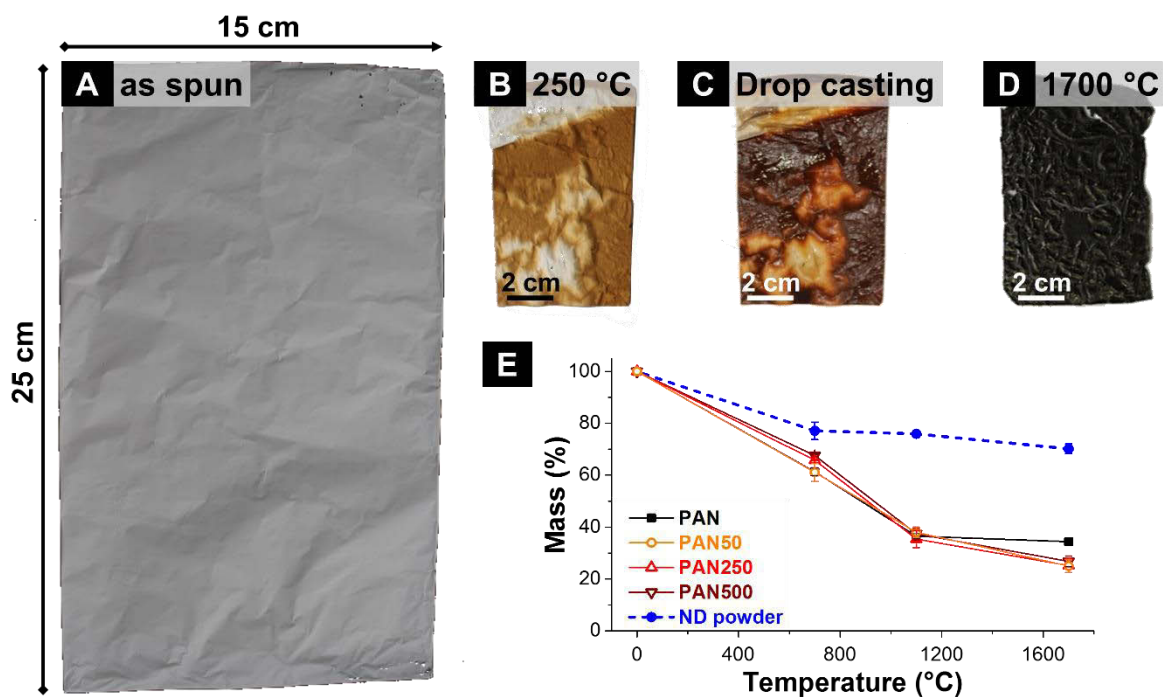


Figure 2. As spun PAN fiber mat on aluminum foil (A). PAN fiber mat after oxidation in air at 250 °C (B), after drop casting of nanodiamonds (5 mass% water dispersion), and after joint thermal annealing in argon at 1700 °C (D). Mass loss for fiber mats with different nanodiamond filling degrees and the nanodiamond powder dependent on the synthesis temperature (E).

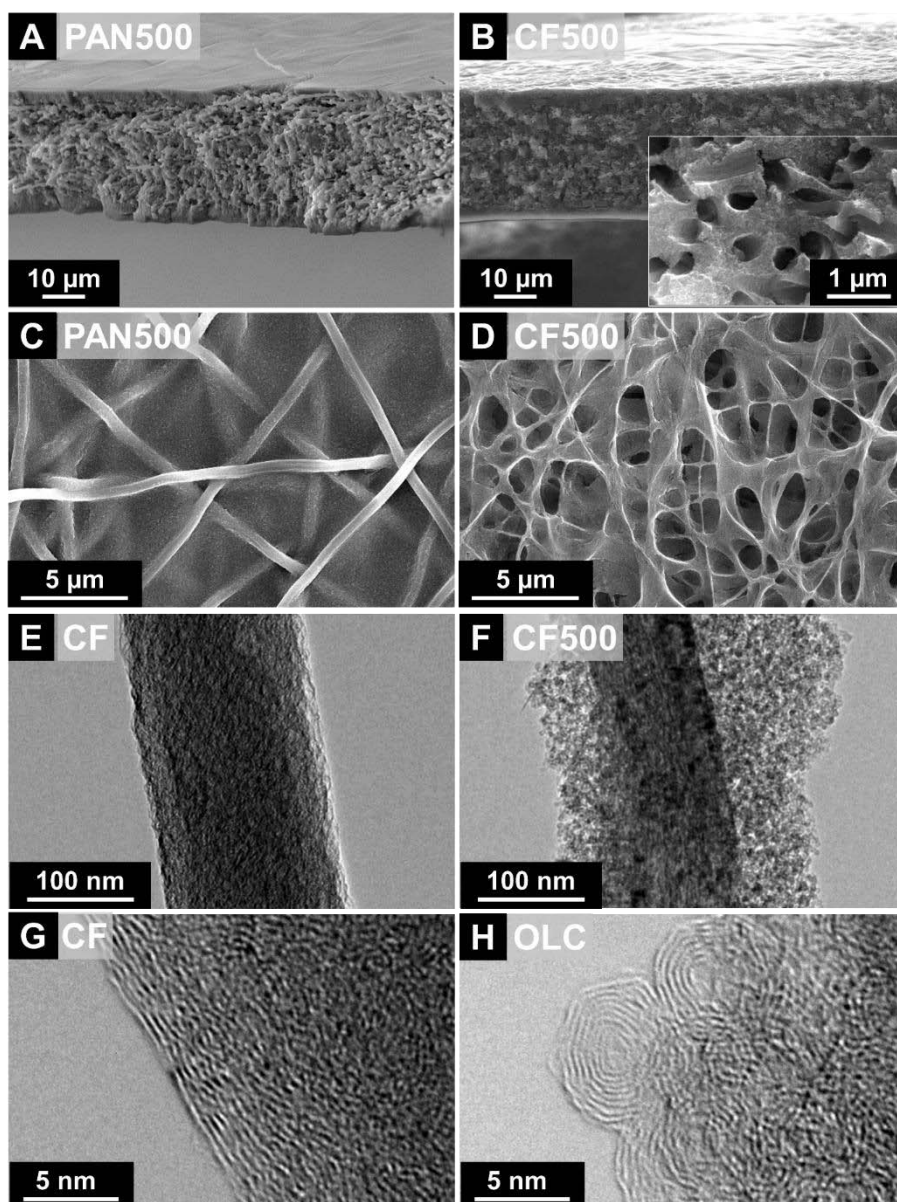


Figure 3. Cross sectional and top view scanning electron micrographs of composites electrodes consisting of oxidized PAN with 500 mass% ND after drop casting (A, C) and after annealing at 1700 °C in argon (B, D). Transmission electron micrographs of carbon fibers (E, G) and the composite electrode with 500 mass% ND (F, H) annealed in argon at 1700 °C.

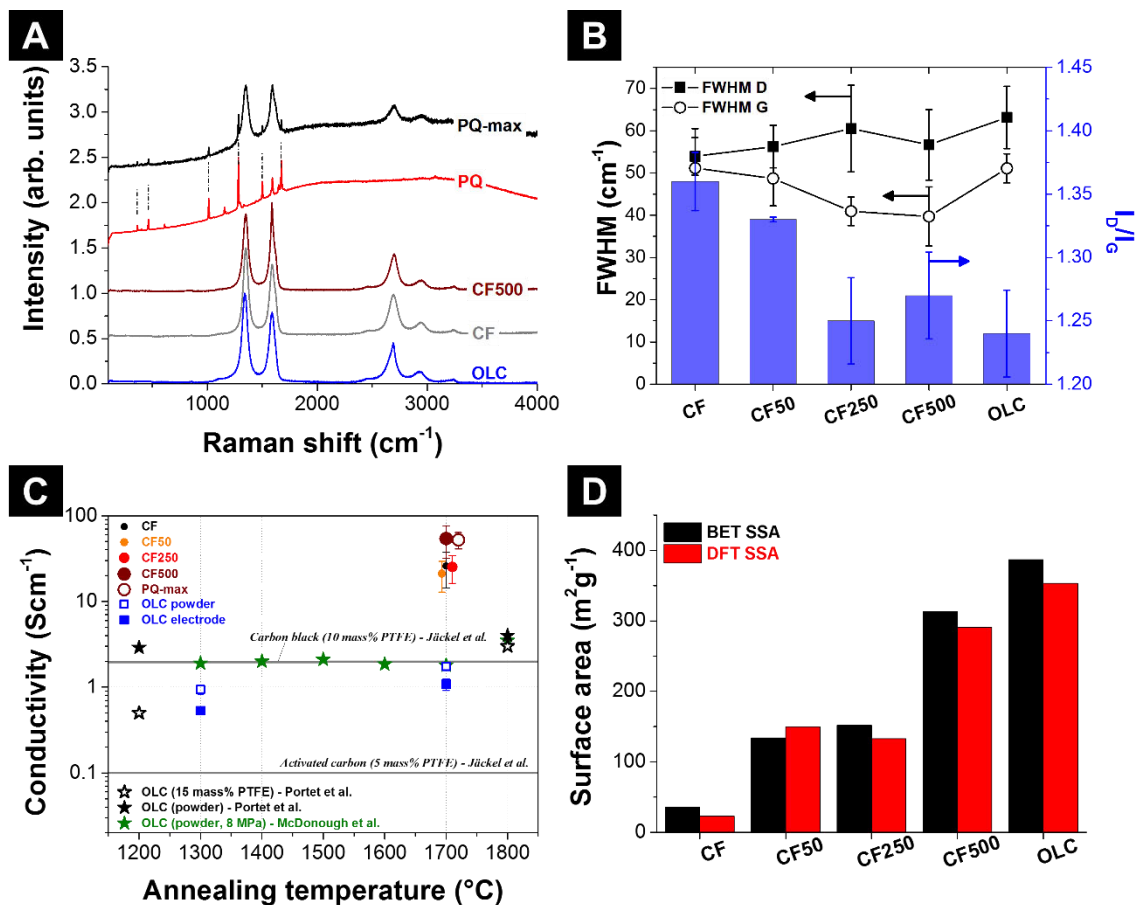


Figure 4. Raman spectra of OLC, CF, the composite electrode with 500 mass% ND (CF500), PQ, and the maximum loading of PQ on CF500 (PQ-max) (A), as well as the FWHM of the D- and the G-mode and the I_D/I_G ratio from Lorentzian peak fitting (B). Conductivities normalized to the electrode thickness for experimental and literature values (C), and the BET and DFT specific surface areas (D). The references in (C) are from Ref. [14, 17, 46].

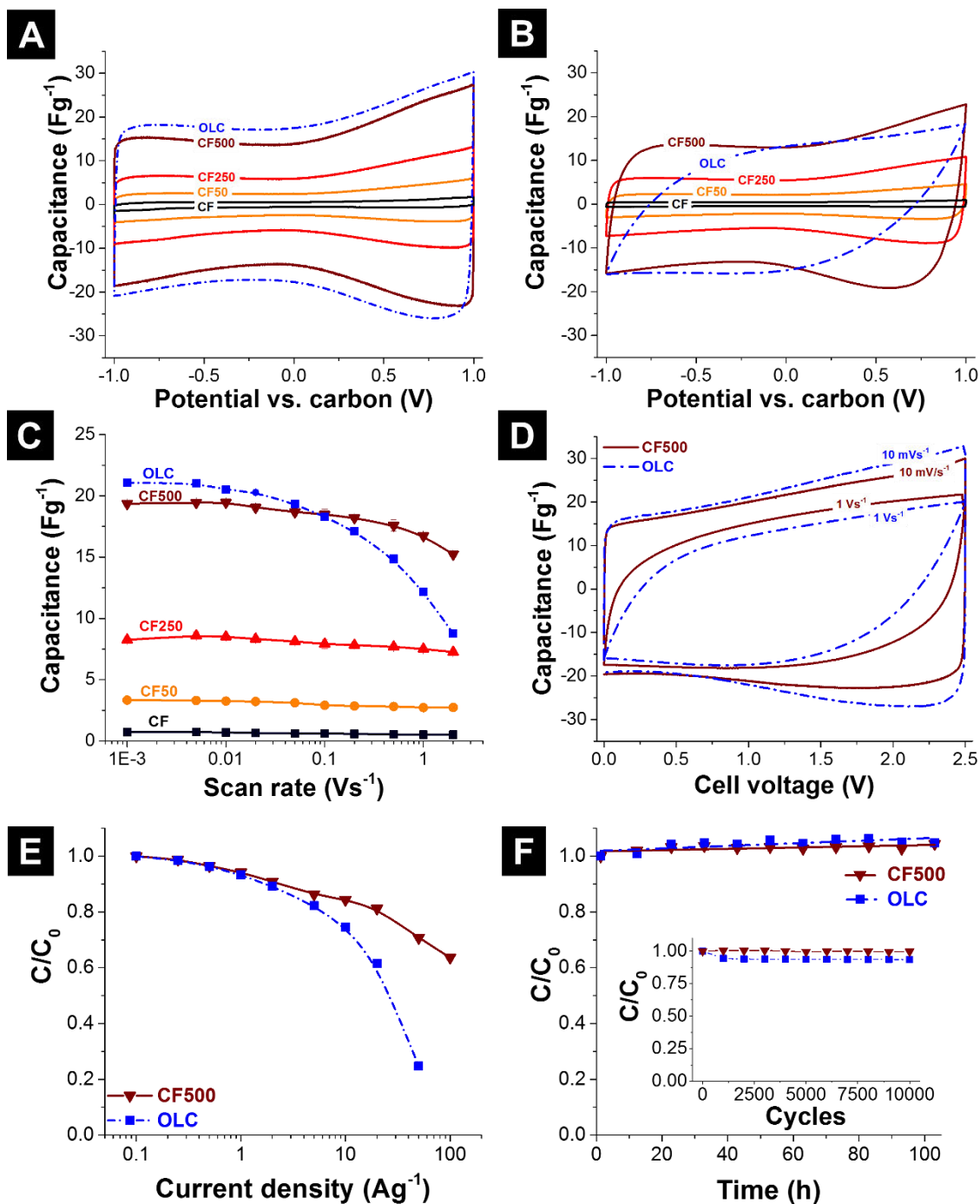


Figure 5. Cyclic voltammograms from -1 V to +1 V vs. carbon for the composite electrodes and the PTFE-bound OLC electrode using a three-electrode set up with a scan rate of 10 mVs⁻¹ (A) and 1 Vs⁻¹ (B). Capacitance measured at 1 V vs. carbon dependent on the scan rate (C). Cyclic voltammograms from 0 V to 2.5 V in a full cell using 10 mVs⁻¹ and 1 Vs⁻¹ for CF500 and the PTFE-bound OLC electrode (D). Rate handling measured in a two electrode setup with galvanostatic cycling with a potential limitation of 2.5 V (E). Long-time voltage floating test using 0.5 Ag⁻¹, 2.5 V potential limitation, and a holding time of 10 h (F). The inset in (F) shows a stability test using 10,000 cyclic voltammograms at 200 mVs⁻¹. All samples were measured in in 1 M TEA-BF₄ in ACN.

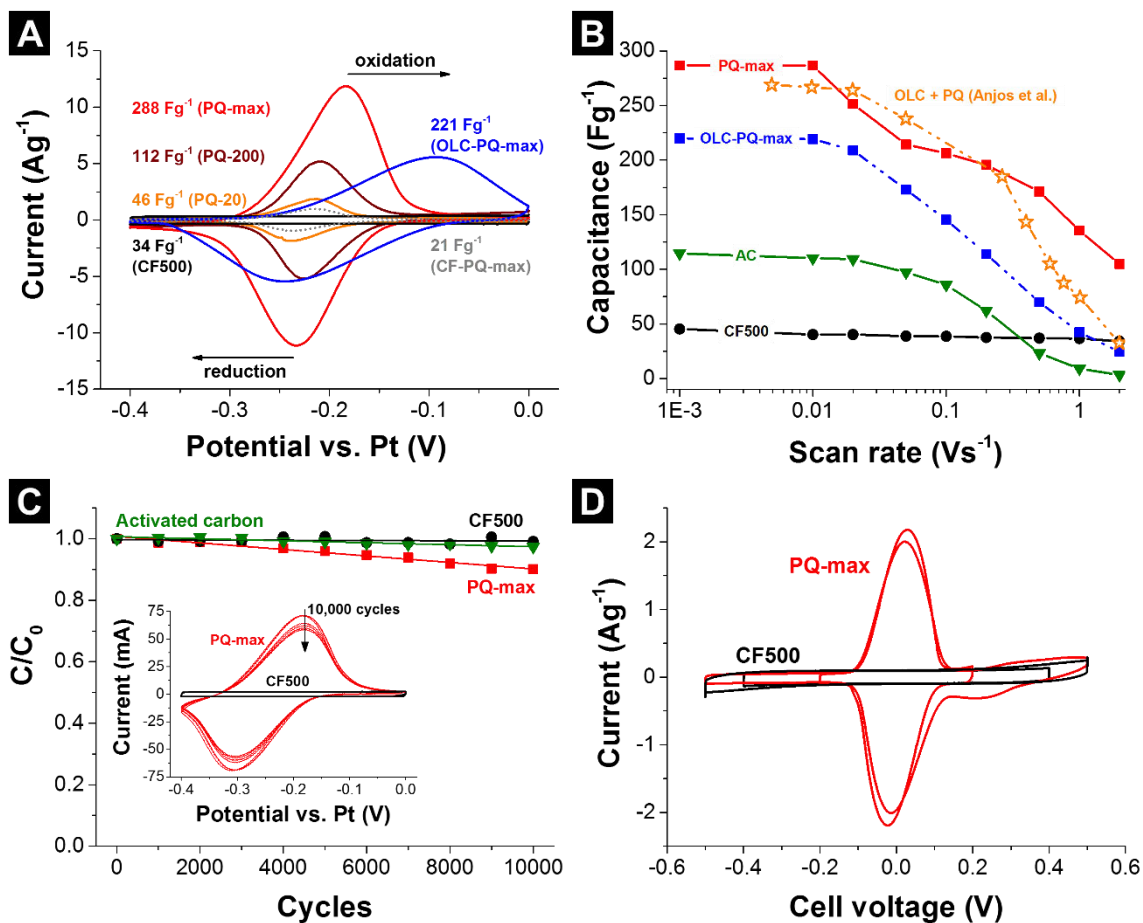


Figure 6. Cyclic voltammograms from -0.4 V to 0 V vs. Pt for the composite electrode CF500, the different loadings with PQ, PTFE-bound OLC, AC electrodes, and the PQ-loaded CF electrode. A three-electrode set up with a platinum wire as reference electrode with a scan rate of 10 mVs^{-1} was used (A). Different scan rates were applied and the capacitance plotted against the scan rate (B). The stability was measured using cyclic voltammetry from -0.4 V to 0 V vs. Pt applying 10,000 cycles at 200 mVs^{-1} (C). Using a full cell the potential window was successively opened up to -0.5 V and +0.5 V for CF500 and PQ-max (D). All samples were measured in aqueous $1 \text{ M H}_2\text{SO}_4$.

Table 1. Capacitance and capacity values for different types of electrodes. All values were determined at 10 mVs^{-1} at 1 V in organic electrolyte and at -0.4 V in aqueous electrolyte using half-cells. Values for pseudocapacitive energy storage are given in Fg^{-1} and mAhg^{-1} .

	Aqueous 1 M H_2SO_4		1 M TEA- BF_4 in ACN	Reference
	Capacitance Fg^{-1}	Capacity mAhg^{-1}	Capacitance Fg^{-1}	
OLC	-	-	21	This work
OLC	-	-	20-27 ⁺	[14]
CF	-	-	1	This work
CF50	-	-	3	This work
CF250	-	-	9	This work
CF500	34	4	20	This work
PQ-20	46	5	-	This work
PQ-200	112	13	-	This work
PQ-max	288	32	-	This work
AC-HQ	280 [‡]	-	-	[30]
PQ-CB-max	257 [†]	-	-	[60]
CF-PQ-max	21	2	-	This work
OLC-PQ-max	221	25	-	This work
OLC-PQ	264 [*]	-	-	[15]

⁺ measured in 1.5 M TEA- BF_4 in ACN.

^{*} measured in three-electrode configuration (half-cell) drop-casted with Nafion on glassy carbon.

[†] measured in 1 M KOH; PQ was electrochemically grafted on carbon black (CB).

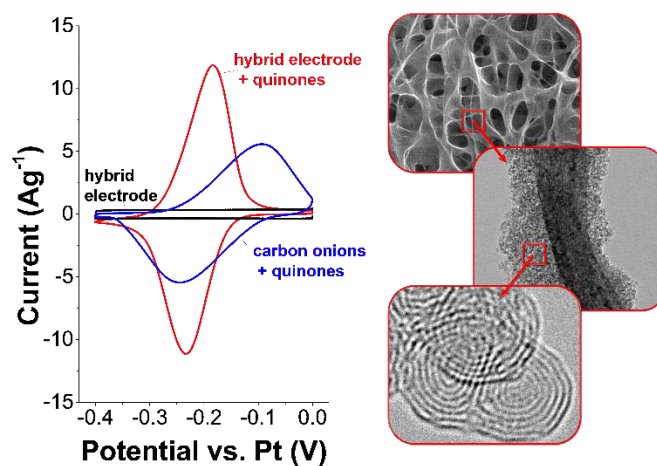
[‡] measured for hydroquinone = 1,4-dihydroxybenzene, not for PQ, using activated carbon (AC).

The rate handling of quinone-decorated carbon supercapacitor electrodes can be increased by a new synthesis method, combining carbon fibers and carbon onions. Polymer-derived, highly conductive, and inter-connected carbon fiber mats are loaded with quinone functionalized carbon onions to build binder-free electrodes with superior rate handling and high capacitance.

Keywords: supercapacitor, carbon onions, quinones, binder-free, rate handling

*Marco Zeiger, Daniel Weingarth, and Volker Presser**

Quinone-decorated onion-like carbon / carbon fiber hybrid electrodes for high rate supercapacitor applications



Supporting Information

Quinone-decorated onion-like carbon / carbon fiber hybrid electrodes for high rate supercapacitor applications

Marco Zeiger, Daniel Weingarh, and Volker Presser*

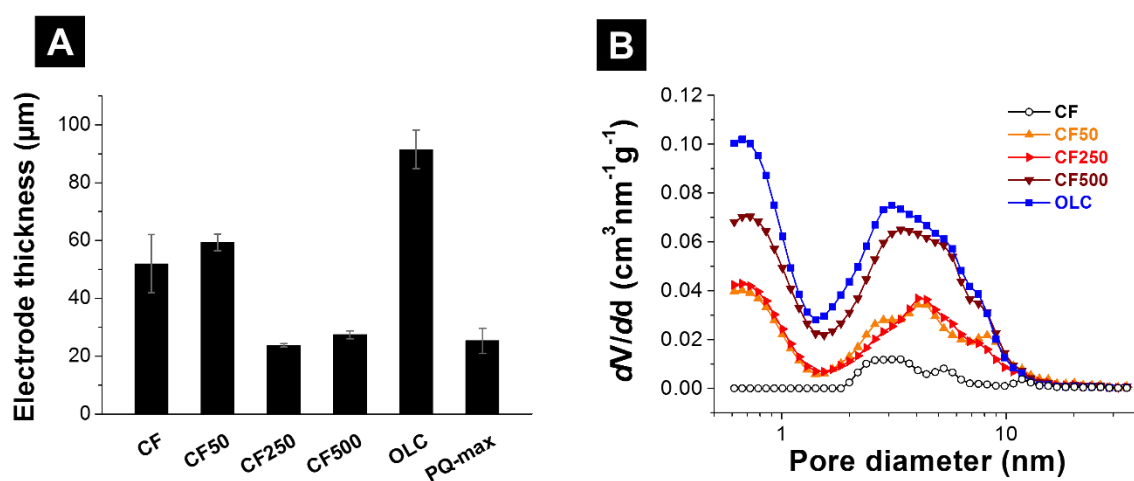


Figure S1. Electrode thickness measured with scanning electron microscopy on cross-sections (A) and pore size distributions from gas sorption analysis and DFT deconvolution (B).

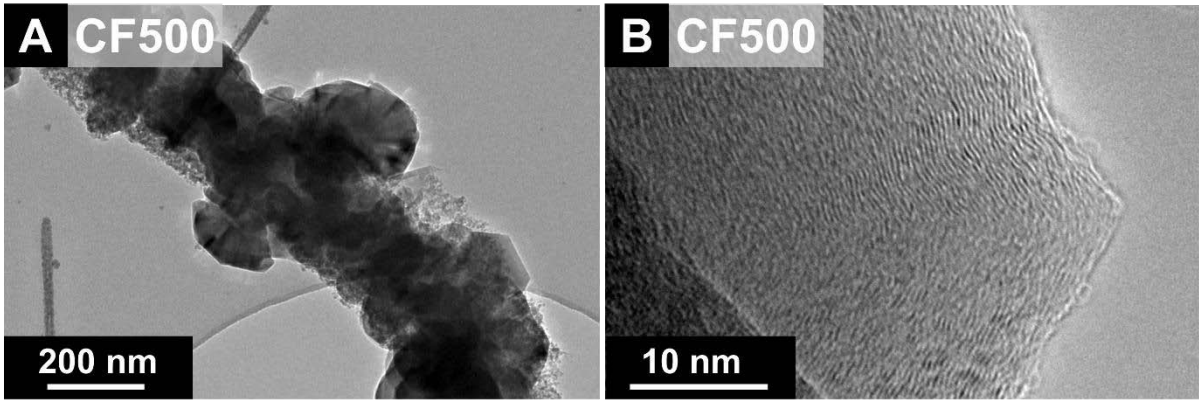


Figure S2. Transmission electron micrographs of the composite electrode CF500.

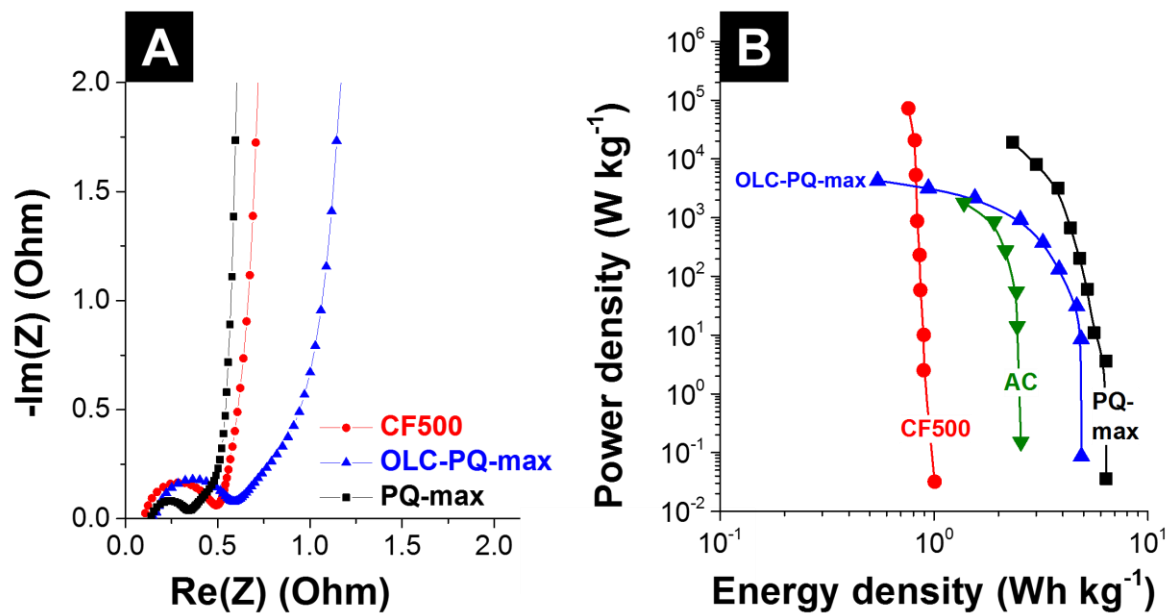


Figure S3. Electrochemical impedance spectroscopy (A) and Ragone plot (B) for CF-500, OLC-PQ-max, and PQ-max samples.